Transition Path Dynamics of a Dielectric Particle in a Bistable Optical Trap

Zijlstra, Niels ; Nettels, Daniel ; Satija, Rohit ; Makarov, Dmitrii E ; Schuler, Benjamin

Abstract: Many processes in chemistry, physics, and biology involve rare events in which the system escapes from a metastable state by surmounting an activation barrier. Examples range from chemical reactions, protein folding, and nucleation events to the catastrophic failure of bridges. A challenge in understanding the underlying mechanisms is that the most interesting information is contained within the rare transition paths, the exceedingly short periods when the barrier is crossed. To establish a model process that enables access to all relevant timescales, although highly disparate, we probe the dynamics of single dielectric particles in a bistable optical trap in solution. Precise localization by high-speed tracking enables us to resolve the transition paths and relate them to the detailed properties of the 3D potential within which the particle diffuses. By varying the barrier height and shape, the experiments provide a stringent benchmark of current theories of transition path dynamics.

DOI: https://doi.org/10.1103/PhysRevLett.125.146001

Transition Path Dynamics of a Dielectric Particle in a Bistable Optical Trap

Niels Zijlstra,[1,*,†] Daniel Nettels,[1,‡] Rohit Satija,[2] Dmitrii E. Makarov,[2,§] and Benjamin Schuler[1,3,‖]
[1]Department of Biochemistry, University of Zurich, 8057 Zurich, Switzerland
[2]Department of Chemistry and Oden Institute for Computational Engineering and Sciences, University of Texas at Austin, Austin, Texas 78712, USA
[3]Department of Physics, University of Zurich, 8057 Zurich, Switzerland

(Received 2 February 2020; accepted 28 August 2020; published 28 September 2020)

Many processes in chemistry, physics, and biology involve rare events in which the system escapes from a metastable state by surmounting an activation barrier. Examples range from chemical reactions, protein folding, and nucleation events to the catastrophic failure of bridges. A challenge in understanding the underlying mechanisms is that the most interesting information is contained within the rare transition paths, the exceedingly short periods when the barrier is crossed. To establish a model process that enables access to all relevant timescales, although highly disparate, we probe the dynamics of single dielectric particles in a bistable optical trap in solution. Precise localization by high-speed tracking enables us to resolve the transition paths and relate them to the detailed properties of the 3D potential within which the particle diffuses. By varying the barrier height and shape, the experiments provide a stringent benchmark of current theories of transition path dynamics.

DOI: 10.1103/PhysRevLett.125.146001

Rate processes in which a system escapes from metastable states via an activation barrier take place on timescales that are long compared to the relaxation dynamics within the states. This separation of timescales allows for the interconversion between states to be approximated in terms of phenomenological chemical kinetics by employing a set of rate coefficients and effectively assuming that the actual interconversion between states is instantaneous [1]. For microscopic systems, a Kramers-type description of the underlying dynamics is more realistic, where the rate coefficients are related to the diffusive motion on an energy surface [2]. This concept has been successfully applied to complex processes such as protein folding and binding [3–5] and provides a conceptual link between the phenomenological kinetics and the underlying molecular dynamics, including the actual process of barrier crossing. These transition paths (TPs) across the barrier contain the most interesting information about the mechanism of the reaction [6], and their investigation has made great progress in the past ten years owing to advances in single-molecule experiments and the concomitant development of theoretical concepts [3,6–15].

Experimental limitations and the complexity of biomolecular systems, however, pose considerable challenges. For instance, the microsecond timescale of typical biomolecular TPs seriously limits the amount of information accessible with experimental time resolution; the choice of reaction coordinates is constrained by the experimentally accessible observables; the actual underlying potentials are often unknown; and data analysis thus requires simplifying assumptions regarding the shape of the energy surface and the nature of the dynamics. To complement the ongoing efforts to overcome such difficulties, our goal here is to provide a simple experimental system that enables all relevant parameters to be extracted directly from the measurements; that covers a broad range of timescales to enable both extensive sampling of the rare transitions and the necessary time resolution to fully resolve TPs; and that allows the shape of the potential to be tuned systematically. Such a system would enable a stringent comparison to simulations and a rigorous test of theoretical concepts at a level of detail that has previously been inaccessible.

To achieve this goal, we employ a spherical dielectric Brownian particle trapped in an optical double-well potential [Fig. 1(a), Supplemental Material [16], Fig. 1]. This configuration has previously been used to test Kramers' theory, e.g., the calculation of rate coefficients based on the shape of the potential [21], the dependence of rates on the damping regime [22], and the transition between ballistic and diffusive motion [23]. The approach is also ideally suited for investigating TPs between the two traps. High-speed camera-based tracking [24–26] enables 3D localization with microsecond time resolution combined with hour-long recording times (Fig. 1, Supplemental Material [16], Fig. 2). The data thus provide both the requisite statistics for obtaining precise transition rates from individual trajectories and the ability to resolve the millisecond TPs [Fig. 1(e)]. Particle position trajectories show the expected bistability of the system in time [Fig. 1(b)]; position autocorrelation functions [Fig. 1(c)] illustrate the eight orders of magnitude accessible in time and reveal both the diffusive dynamics within the traps and the

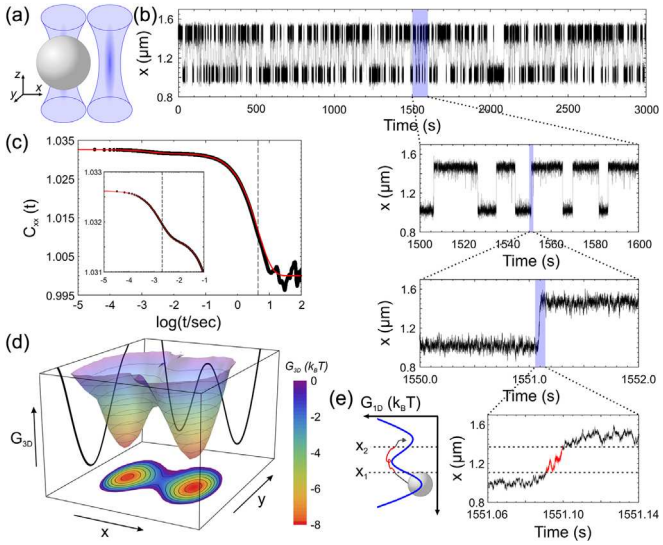

FIG. 1. Transition paths in the bistable optical trap. (a) Schematic of a microsphere (fused silica, radius ∼270 nm) in a bistable trap formed by two laser foci (wavelength 485 nm) separated by ∼450 nm. The z coordinate is deduced from the ring pattern of the diffraction-limited image of the bead with a precision of ∼50 nm; its symmetry center yields the x and y coordinates with a precision of ∼25 nm. See the Supplemental Material [16] for technical details. (b) A trajectory along x, the interfocus axis, with enlargements at increasing time resolutions. (c) The position autocorrelation function C_{xx} reveals diffusive dynamics within the traps (correlation time 2.2 ± 0.1 ms) and kinetics of transitions between them ($k^{-1} = 4.4 \pm 0.1$ s). The red line is a fit with $C_{xx}(t) = \langle x \rangle^2 e^{-kt} + (k_B T/\kappa) e^{-(D\kappa/k_B T)t} + 1$, where $\langle x \rangle$ is the trap separation, k the transition rate between the wells, κ the average curvature of the free energy at the bottom of the two wells, and D the diffusion constant. (d) The 3D potential, G_{3D}, extracted from the distribution of the particle positions (color projection). (e) Illustration of a TP (red) between boundaries x_1 and x_2 along the one-dimensional free-energy profile, $G_{1D}(x)$ (duration in this example 8.8 ms).

kinetics of transitions between them. From the distribution $P_{3D}(\mathbf{r})$ of the particle's position $\mathbf{r} = (x, y, z)$ based on 10^6 to 10^8 images per trajectory, the three-dimensional free-energy landscape is readily reconstructed as $G_{3D}(\mathbf{r}) = -k_B T \ln P_{3D}(\mathbf{r})$, where k_B is Boltzmann's constant and T is temperature [Fig. 1(d)]. The diffusion coefficient D of each particle was determined from its mean-squared displacement at short times [21] (Supplemental Material [16], Fig. 3). Notably, variations in particle shape and size lead to variations by ∼10% in D; similarly, such particle-to-particle variations and the possible influence of Mie resonances [27] at a given shape and radiant flux of the laser beams lead to clearly detectable differences in the shapes of the potentials (Supplemental Material [16], Figs. 3 and 4). However, since the potentials are obtained by Boltzmann inversion for each particle and laser power individually, all these contributions are accounted for and do not need to be modeled explicitly. By adjusting the

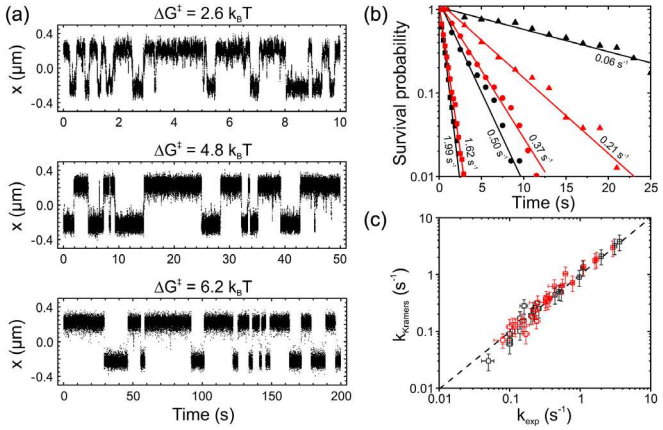

FIG. 2. Transition rates and Kramers' theory. (a) Examples of particle trajectories projected on the interfocus axis x [cf. Fig. 1 (a)] with different barrier heights and transition frequencies. (b) Survival probability distributions in the traps fitted with exponential decays (lines) yield the interwell transition rate coefficients. Since the potentials are never perfectly symmetric, transitions in the two directions are analyzed separately (black: x increasing; red: x decreasing, identical symbols: same particle). (c) Comparison of the transition rate coefficients according to Kramers' theory, k_{Kramers}, with measured values, k_{exp} (black: x increasing; red: x decreasing; identity line: dashed). Error bars for k_{Kramers} result from uncertainties in the barrier and well curvatures and barrier heights, error bars in k_{exp} from uncertainties in the fits of the survival probability distributions (b).

laser power, we can tune the barrier height systematically between ∼2 and 8 k_BT, corresponding to a hundredfold change in transition rate coefficients (Fig. 2). The accessible range of rates is limited at low laser power by the loss of persistent trapping, and at high laser power by insufficient sampling of the potential in the transition region.

As the friction force on the particle obeys Stokes' law and is proportional to its velocity, we expect the particle dynamics to be described by a three-dimensional Langevin equation in the potential $G_{3D}(\mathbf{r})$. Since the particle's motion is overdamped [21,22], inertial contributions can be neglected [2]. The kinetics of transitions between the wells can then be described using Langer's rate theory of multidimensional diffusive barrier crossing [28]. The symmetry of the potential suggests that the reaction coordinate of this process coincides with the x axis along the interfocus distance (Fig. 1); moreover, because of the symmetry of the potential at stationary points, the dynamics along x are decoupled from those along y and z near the barrier saddle. As a result, Kramers model [29] of one-dimensional diffusive barrier crossing in the 1D free-energy landscape $G_{1D}(x) = -k_B T \ln P_{1D}(x)$ is sufficient, where $P_{1D}(x) = \iint P_{3D}(\mathbf{r}) dy dz$ is the probability distribution of the position along x. The Kramers rate for crossing a barrier of height $\Delta G^{\ddagger}$ is

$$k_{\mathrm{Kramers}} = (D\sqrt{\kappa_b \kappa_w}/2\pi) e^{-\Delta G^{\ddagger}/k_B T}, \qquad (1)$$

where κ_b and κ_w are the curvatures of the potential $G_{1D}(x)$ at the top of its barrier and at the bottom of the initial potential well, respectively. Note that D is independent of position in our experimental system. To test the applicability of the Kramers' theory, we extracted transition rate coefficients from the measured particle trajectories projected on x, assuming first-order kinetics between the two states, and compared them to the values from a Kramers model (Fig. 2), using $G_{1D}(x)$ (Supplemental Material [16], Fig. 5) and D obtained for the respective individual particles from their mean-square displacements after short times (see the Supplemental Material [16]). The agreement [Fig. 2(c)] confirms the applicability of Kramers' theory [21] and illustrates the high data quality available from individual particle trajectories.

Examples of transitions from one trap to the other are shown in Fig. 3(a), projected on the xy and xz planes, and along x. TPs are the segments of the trajectory where the particle continuously dwells in the transition region between the two potential wells, having entered it from one well and exiting to the other [red segments in Fig. 3(a)]. For trajectories in 3D, we defined the boundaries of the transition regions as isoenergetic surfaces enclosing the potential minima, $G_{3D}(\mathbf{r}) = E_1$ and $G_{3D}(\mathbf{r}) = E_2$, where E_1 and E_2 were chosen as the energy values halfway between the barrier top and the bottom of the respective minima of the potential, $G_{3D}(x, \langle y \rangle, \langle z \rangle)$. For 1D projections, $x(t)$, the boundaries correspond to the values x_1 and x_2 defined by $G_{1D}(x) = E_1$ and $G_{1D}(x) = E_2$, with E_1 and E_2 chosen halfway between the barrier top and the respective minima of $G_{1D}(x)$. The transition region then coincides with the interval $[x_1, x_2]$. Although the TPs identified in 3D differ from those identified in 1D or 2D, the mean TP times in 1D are on average only ~15% shorter than in 3D, indicating robustness to the dimensionality of the analysis used (Supplemental Material [16], Fig. 6).

The average TP times $\langle \tau_{\mathrm{TP}} \rangle$ are well reproduced by Brownian dynamics simulations in the corresponding potentials, over a wide range of barrier heights and for different choices of TP boundaries [Fig. 3(b)]. The agreement is similarly good for the numerical solution of the diffusion problem using the detailed shapes of the potentials [31]. Remarkably, $\langle \tau_{\mathrm{TP}} \rangle$ for all but the lowest barriers are almost as well reproduced by the Szabo approximation [3,6,30], according to which $\langle \tau_{\mathrm{TP}} \rangle = (k_B T / D\kappa_b) \ln(2e^{\gamma} \Delta G^* / k_B T)$, where ΔG^* is the barrier height measured relative to the values of $G_{1D}(x)$ at the TP boundaries, and $\gamma \approx 0.577$ is Euler's constant. This relation, derived for diffusive crossing of a symmetric parabolic 1D barrier with $\Delta G^* \gg k_B T$ [30], is commonly used for the analysis of experimentally measured biomolecular TP times [6,10], where information about the shape of the potential is often unavailable. Figure 3(c) illustrates an important observation: in contrast to the transition rates, which depend exponentially on the activation free energy [Eq. (1), Fig. 2(c)], TP times are much

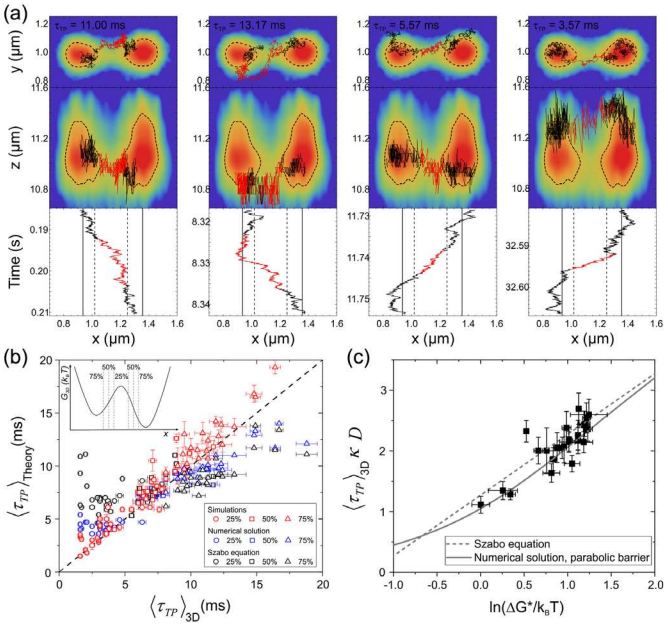

FIG. 3. Quantifying TP times and dependence on barrier height. (a) Examples of TPs projected on the xy and xz planes (top), with the free energy shown by the color scale as in Fig. 1. Dashed lines indicate the TP boundary in the xy and xz planes; red trajectory segments indicate the TPs identified in 3D. The bottom panels show the TPs projected onto the x axis. Solid vertical lines indicate trap centers, dashed lines TP boundaries along x. (b) Measured average TP times for each particle compared to the results from 3D-Brownian dynamics simulations (red symbols), to the numerical solution of the 1D diffusion problem on the measured potential of mean force (blue symbols), and to the results from theory using the Szabo equation [3,6,30] (black symbols, averages of ΔG^* in both directions of the transition were used) with different TP boundaries (see inset and legend). (c) Average TP times for each particle using TP boundaries at 50% [see inset in (b)] compared with the Szabo approximation (gray dashed line) and the numerical solution (solid gray line) using the curvatures of the experimentally determined potentials and the diffusion coefficient averaged over all measurements.

less sensitive to the barrier height. The dependence of $\langle \tau_{\mathrm{TP}} \rangle$ on ΔG^* is also well described by the Szabo equation.

The time resolution of our experiment allows us to quantify not only average TP times but also their distributions and the dependence on the barrier height for each particle (Fig. 4 and Supplemental Material [16], Fig. 7). As expected for diffusive barrier crossing, we observe peaked asymmetric distributions with exponential tails [31,32]. The distributions are compared with those predicted by three theoretical models: Brownian dynamics simulations using $G_{3D}(\mathbf{r})$ and D from the experiments; the numerical solution for diffusive dynamics in $G_{1D}(x)$ [31]; and the analytical approximation for the diffusive dynamics across a high 1D parabolic barrier [32]. All three approaches are in remarkably good agreement with experiment for barriers with $\Delta G^* > 3k_b T$ [Fig. 4(a)]. For smaller barriers, the analytical approximation deviates from the experimental

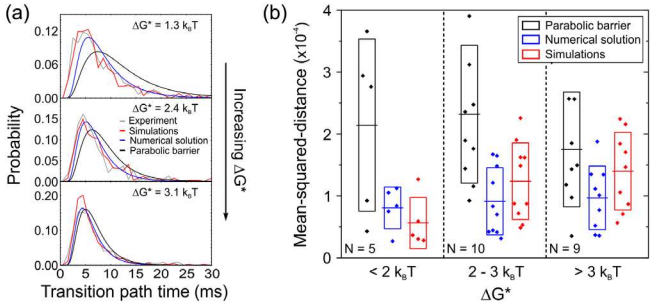

FIG. 4. Transition path time distributions for different barrier heights. (a) Examples of TP time distributions from measurements of individual particles (barrier heights given in each panel). Experimentally determined distributions (gray) are compared to 3D Brownian dynamics simulations (red), the numerical solution for 1D diffusion in the potential (blue) [31], and the analytical approximation for a parabolic barrier (black) [32]. (b) Mean-squared-distance (χ^2) between experimental and theoretical TP time distributions, divided into low ($\Delta G^* < 2k_bT$), intermediate ($2k_bT < \Delta G^* < 3k_bT$), and high ($\Delta G^* > 3k_bT$) barrier heights ΔG^* (averaged in both directions). (Symbols: individual measurements; solid line: average; rectangles: standard deviation of mean-squared-distance; N: number of distributions, each from an individual particle, contributing to each class.)

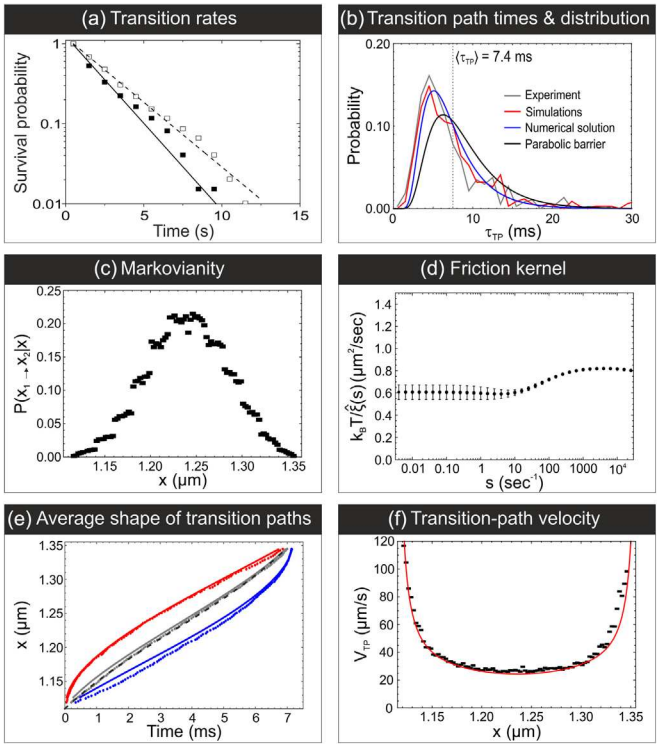

FIG. 5. Detailed information on transition paths. The dynamics of dielectric particles in a bistable optical trap provides a wide range of information and direct comparison to theory, including (a) transition rates from dwell-time distributions, (b) distributions of TP times, (c) the Markovianity of the process [33], (d) the friction memory kernel [Eq. (10) in Ref. [34]], (e) the average shape of the TPs (circles: experiment, lines: theory; red and blue: average first and last crossing times [35], gray: average TP shape [Eq. (4) in Ref. [36]]. Interestingly, the average TP is nearly indistinguishable from the most probable TP [37] estimated using the harmonic approximation [Eq. (6) in Ref. [38]], dashed black line. (f) The transition-path velocity as defined in Ref. [39] [Eq. (5)] (black symbols) compared with the theoretical prediction [red line, Eq. (17) in Ref. [39]]. See main text and the Supplemental Material [16] for details and equations.

data, whereas 3D simulations and the 1D numerical solution agree to within error down to very low barriers.

The TP time is an important property, but much more information can be gleaned from the observed barrier crossing dynamics. For instance, most of the analyses of TP times in single-molecule experiments have relied on the *a priori* assumption of diffusive dynamics. However, this assumption (which does not necessarily hold for molecular reaction coordinates) can be tested directly here: first, we applied the recently proposed Markovianity test [33], which computes the conditional probability $P(x_1 \to x_2|x)$ that the system at point x (with $x_1 < x < x_2$) is on a TP from boundary x_1 to boundary x_2. For a Markov process, this probability peaks at a value of 0.25, whereas memory effects reduce its maximum value. In our experiments, the observed barrier crossing dynamics indeed closely approach Markovianity [Fig. 5(c)]. The residual deviation from 0.25 is presumably caused by the rare misidentification of fast TPs (Supplemental Material [16], Fig. 11).

Second, we applied a more general dynamic model to the observed $x(t)$ in which the friction force is not simply proportional to the instantaneous velocity $\dot{x}(t)$ but depends on past velocities, $F_{\rm fr} = -\int_{-\infty}^{t} \xi(t-t')\dot{x}(t')dt'$. The friction memory kernel, $\xi(t)$, can be reconstructed directly from the observed trajectories [34]. The Laplace transform of $\xi(t)$, $\hat{\xi}(s) = \int_0^\infty \xi(t)e^{-st}dt$, is close to a constant, $\hat{\xi}(s) = \xi_0$, in the experimentally accessible frequency range [Fig. 5(d)], which means that $\xi(t)$ is well approximated by a delta function, and $F_{\rm fr}$ is simply proportional to the instantaneous velocity, $F_{\rm fr} = -\xi_0\dot{x}$, providing direct evidence for diffusive dynamics. Moreover, the resulting estimate of D based on the Einstein relation, $D = k_BT/\xi_0$, agrees with the values from the mean square displacement and the position correlation function (Supplemental Material [16], Fig. 3).

Finally, we quantified the average shape of the TPs [35,36,38] [Fig. 5(e)] and the transition-path velocity profile [33], $v_{\rm TP}(x)$ [Fig. 5(f)], which characterizes the dynamics of barrier crossing in terms of the time derivative of the average shape. Consistent with the model of diffusive crossing of a parabolic barrier, these profiles are monotonic functions of the coordinate with a minimum at the barrier top [35,38,39].

In summary, high-speed tracking of dielectric particles in a bistable optical trap thus provides the opportunity to resolve TPs of a diffusive barrier crossing process with great precision and to quantify their properties in unprecedented detail. A key strength of the approach is that the parameters determining the dynamics—the 3D shape of the

potential and the diffusion coefficient of the particle—can be extracted directly from the experimental data, essentially without simplifying assumptions. The results thus offer a stringent experimental benchmark for the theoretical concepts used in the investigation of TPs [3,6–14]. Given that applying a broad range of analysis tools to our experimental model system allowed us to correctly recover details of its underlying dynamics without making any prior assumptions regarding, e.g., the validity of the Kramers picture, our results are very encouraging for the field of single-molecule biophysics, as we expect that the same approach can be used to infer accurate models of barrier crossing dynamics directly from biomolecular transition paths. Experiments of this type and their analysis may help to address challenging open questions regarding TPs, such as the discrepancy between barrier heights using different types of analysis [9], or the observation of TP velocity profiles with a maximum instead of a minimum [40].

We thank Attila Szabo for many valuable discussions and comments on the manuscript. This work was supported by the Swiss National Science Foundation (to B. S.), by the Forschungskredit of the University of Zurich (to N. Z.), by the Robert W. Welch Foundation (Grant No. F-1514 to D. E. M.) and by the U.S. National Science Foundation (Grant No. CHE 1566001 to D. E. M.).

*Present address: Physical and Synthetic Biology, Faculty of Biology, Ludwig-Maximilans-Universität München, Großhadernerstrasse 2-4, 82152 Planegg-Martinsried, Germany
†n.zijlstra@lmu.de
‡nettels@bioc.uzh.ch
§makarov@cm.utexas.edu
‖schuler@bioc.uzh.ch

[1] N. G. van Kampen, *Stochastic Processes in Physics and Chemistry* (Elsevier, New York, 1992).
[2] P. Hänggi, P. Talkner, and M. Borkovec, Reaction-rate theory: fifty years after Kramers, Rev. Mod. Phys. **62**, 251 (1990).
[3] H. S. Chung, J. M. Louis, and W. A. Eaton, Experimental determination of upper bound for transition path times in protein folding from single-molecule photon-by-photon trajectories, Proc. Natl. Acad. Sci. U.S.A. **106**, 11837 (2009).
[4] D. Shoup and A. Szabo, Role of diffusion in ligand binding to macromolecules and cell-bound receptors, Biophys. J. **40**, 33 (1982).
[5] R. B. Best and G. Hummer, Diffusion models of protein folding, Phys. Chem. Chem. Phys. **13**, 16902 (2011).
[6] G. Hummer, From transition paths to transition states and rate coefficients, J. Chem. Phys. **120**, 516 (2004).
[7] P. G. Bolhuis, D. Chandler, C. Dellago, and P. L. Geissler, Transition path sampling: Throwing ropes over rough mountain passes, in the dark, Annu. Rev. Phys. Chem. **53**, 291 (2002).
[8] D. E. Makarov, *Single Molecule Science: Physical Principles and Models* (CRC Press, Boca Raton, 2015).
[9] K. Neupane, D. A. N. Foster, D. R. Dee, H. Yu, F. Wang, and M. T. Woodside, Direct observation of transition paths during the folding of proteins and nucleic acids, Science **352**, 239 (2016).
[10] H. S. Chung and W. A. Eaton, Protein folding transition path times from single molecule FRET, Curr. Opin. Struct. Biol. **48**, 30 (2018).
[11] R. B. Best and G. Hummer, Microscopic interpretation of folding phi-values using the transition path ensemble, Proc. Natl. Acad. Sci. U.S.A. **113**, 3263 (2016).
[12] K. Lindorff-Larsen, S. Piana, R. O. Dror, and D. E. Shaw, How fast-folding proteins fold, Science **334**, 517 (2011).
[13] F. Sturzenegger, F. Zosel, E. D. Holmstrom, K. J. Buholzer, D. E. Makarov, D. Nettels, and B. Schuler, Transition path times of coupled folding and binding reveal the formation of an encounter complex, Nat. Commun. **9**, 4708 (2018).
[14] N. Q. Hoffer and M. T. Woodside, Probing microscopic conformational dynamics in folding reactions by measuring transition paths, Curr. Opin. Chem. Biol. **53**, 68 (2019).
[15] E. Weinan and E. Vanden-Eijnden, Transition-path theory and path-finding algorithms for the study of rare events, Annu. Rev. Phys. Chem. **61**, 391 (2010).
[16] See the Supplemental Material at http://link.aps.org/supplemental/10.1103/PhysRevLett.125.146001 for methods and Supplemental Figures, which includes Refs. [17–20].
[17] A. Jain, A. H. Yang, and D. Erickson, Gel-based optical waveguides with live cell encapsulation and integrated microfluidics, Opt. Lett. **37**, 1472 (2012).
[18] A. Berezhkovskii and A. Szabo, One-dimensional reaction coordinates for diffusive activated rate processes in many dimensions, J. Chem. Phys. **122**, 014503 (2005).
[19] D. E. Makarov, Interplay of non-Markov and internal friction effects in the barrier crossing kinetics of biopolymers: Insights from an analytically solvable model, J. Chem. Phys. **138**, 014102 (2013).
[20] R. F. Grote and J. T. Hynes, The stable states picture of chemical reactions. II. Rate constants for condensed and gas phase reaction models, J. Chem. Phys. **73**, 2715 (1980).
[21] L. I. McCann, M. Dykman, and B. Golding, Thermally activated transitions in a bistable three-dimensional optical trap, Nature (London) **402**, 785 (1999).
[22] L. Rondin, J. Gieseler, F. Ricci, R. Quidant, C. Dellago, and L. Novotny, Direct measurement of Kramers turnover with a levitated nanoparticle, Nanotechnology **12**, 1130 (2017).
[23] T. Li, S. Kheifets, D. Medellin, and M. G. Raizen, Measurement of the instantaneous velocity of a Brownian particle, Science **328**, 1673 (2010).
[24] B. M. Lansdorp, S. J. Tabrizi, A. Dittmore, and O. A. Saleh, A high-speed magnetic tweezer beyond 10,000 frames per second, Rev. Sci. Instrum. **84**, 044301 (2013).
[25] A. Huhle, D. Klaue, H. Brutzer, P. Daldrop, S. Joo, O. Otto, U. F. Keyser, and R. Seidel, Camera-based three-dimensional real-time particle tracking at kHz rates and Ångstrm accuracy, Nat. Commun. **6**, 5885 (2015).
[26] R. Parthasarathy, Rapid, accurate particle tracking by calculation of radial symmetry centers, Nat. Methods **9**, 724 (2012).

[27] A. B. Stilgoe, T. A. Nieminen, G. Knöner, N. R. Heckenberg, and H. Rubinsztein-Dunlop, The effect of Mie resonances on trapping in optical tweezers, Opt. Express **16**, 15039 (2008).
[28] J. Langer, Statistical theory of the decay of metastable states, Ann. Phys. (N.Y.) **54**, 258 (1969).
[29] H. A. Kramers, Brownian motion in a field of force and the diffusion model of chemical reactions, Physica **7**, 284 (1940).
[30] H. S. Chung and I. V. Gopich, Fast single-molecule FRET spectroscopy: theory and experiment, Phys. Chem. Chem. Phys. **16**, 18644 (2014).
[31] S. Chaudhury and D. E. Makarov, A harmonic transition state approximation for the duration of reactive events in complex molecular rearrangements, J. Chem. Phys. **133**, 034118 (2010).
[32] B. W. Zhang, D. Jasnow, and D. M. Zuckerman, Transition-event durations in one-dimensional activated processes, J. Chem. Phys. **126**, 074504 (2007).
[33] A. M. Berezhkovskii and D. E. Makarov, Single-molecule test for Markovianity of the dynamics along a reaction coordinate, J. Phys. Chem. Lett. **9**, 2190 (2018).
[34] R. Satija and D. E. Makarov, Generalized Langevin equation as a model for barrier crossing dynamics in biomolecular folding, J. Phys. Chem. B **123**, 802 (2019).
[35] W. K. Kim and R. R. Netz, The mean shape of transition and first-passage paths, J. Chem. Phys. **143**, 224108 (2015).
[36] D. E. Makarov, Shapes of dominant transition paths from single-molecule force spectroscopy, J. Chem. Phys. **143**, 194103 (2015).
[37] P. Faccioli, M. Sega, F. Pederiva, and H. Orland, Dominant Pathways in Protein Folding, Phys. Rev. Lett. **97**, 108101 (2006).
[38] P. Cossio, G. Hummer, and A. Szabo, Transition paths in single-molecule force spectroscopy, J. Chem. Phys. **148**, 123309 (2018).
[39] A. M. Berezhkovskii and D. E. Makarov, Communication: Transition-path velocity as an experimental measure of barrier crossing dynamics, J. Chem. Phys. **148**, 201102 (2018).
[40] K. Neupane, N. Q. Hoffer, and M. T. Woodside, Measuring the Local Velocity along Transition Paths During the Folding of Single Biological Molecules, Phys. Rev. Lett. **121**, 018102 (2018).